Self-Assembled Monolayers Based on Pd-Containing Organometallic Thiols: Preparation and Structural Characterization

ARTICLE *in* THE JOURNAL OF PHYSICAL CHEMISTRY A · SEPTEMBER 2009

Impact Factor: 2.69 · DOI: 10.1021/jp904865k · Source: PubMed

Self-Assembled Monolayers Based on Pd-Containing Organometallic Thiols: Preparation and Structural Characterization†

Rosa Vitaliano,† Ilaria Fratoddi,† Iole Venditti,† Giuseppina Roviello,‡ Chiara Battocchio,*,§ Giovanni Polzonetti,§ and Maria Vittoria Russo†

Department of Chemistry, University of Rome "La Sapienza" P. le A. Moro, 5- 00185, Rome, Italy, Department of Chemistry, University of Napoli "Federico II", Complesso di Monte Sant'Angelo, Via Cintia, 80126 Napoli, Italy, Department of Physics, INSTM, CNISM and CISDiC, University of Rome "Roma Tre" via della Vasca Navale 84 00146 Rome, Italy

Received: May 25, 2009; Revised Manuscript Received: July 16, 2009

Multilayers and self-assembled monolayers of on-purpose-prepared organometallic thiolates, *trans*-[$Pd(PBu_3)_2(SCOCH_3)_2$], *trans*-[$(C_6H_5C{\equiv}C)Pd(PBu_3)_2(SCOCH_3)$], and *trans*,*trans*-[$(CH_3COS)Pd(PBu_3)_2$-$(C{\equiv}C-C_6H_4-C_6H_4-C{\equiv}C)(PBu_3)_2Pd(SCOCH_3)$] were deposited onto gold surfaces. High-resolution X-ray photoelectron spectroscopy and near-edge X-ray absorption fine structure measurements allowed us to assess the anchoring of the organometallic thiols onto gold substrates; the interaction occurring at the interface; and their molecular orientation on the surface with tilt angles of about 30°−40°, depending on the investigated molecule. The molecule packing density/coverage was also assessed.

1. Introduction

In recent years, scientific research has been devoted to the emerging field of the preparation of nanostructured materials for applications ranging from nanomedicine to nanoelectronics,[1] and the formation and control of self-assembled monolayers (SAMs) of organic thiols on several substrates, such as noble metals, have attracted interest in the research community.[2,3] Several efforts devoted to in-depth theoretical understanding of the geometric and electronic structure of self-assembled thiols have been developed to provide information on properties of SAMs[4] in view of potential applications of these systems.[5] SAM structures are governed by several factors, among them the nature of the substrate and adsorbate, the interaction between the molecules and the substrate, and the intramolecular interactions. SAM properties are determined by a combination of the molecular structure and the SAM organization. A number of studies have been reported for aromatic thiol SAMs on gold.[6] The molecular orientation and packing density strongly depends on the interplay between the sulfur−gold and the intermolecular lateral interactions between the SAM constituents; in this context, several works report that the packing of the organic groups can be improved by stacking interactions between the aromatic rings in the adjacent adsorbates, thus increasing the packing density.[7] In this regard, oligo(aryleneethynylene)s represent an attractive class of molecules[8,9] because of their rigid-rod structure, and although they show a low barrier to rotation along the aryl-ethynyl bond,[10,11] some of these molecules with terminal thiol groups have been integrated into electronic circuits.[12]

The synthesis of new oligo(aryleneethynylene) molecular wires of ∼4 nm length scale with terminal thiolates has been recently reported and used for the preparation of self-assembled monolayers on gold substrates.[13] Among others, organometallic oligomers and polymers have recently received great interest due to the possibility of coupling the chemical, electronic, optical, and redox properties of transition metal complexes to those of organic spacers.[14−19] These materials show useful properties for applications in modern technology,[20] and molecular models of long-chain organometallic polymers allow in-depth understanding and modulation of the molecular structure and electronic properties of the corresponding polymers.[21] Moreover, if the oligomers possess a thiol group at both ends as an anchoring unit, the bridging of two surfaces/electrodes is possible,[22] and linearly structured π-conjugated organic and inorganic building blocks can be used as connecting units. The properties of such molecules strongly depend on the nature of the redox moiety and the appropriate connecting spacer.[23] Organic thiols have received a great deal of attention,[24] and the use of redox-active organometallic complexes offers perspectives for the design and preparation of self-assembled monolayers.[25] For example, the fabrication and characterization of fully organometallic multilayer thin films composed of poly(ferrocenylsilane) polyanions and polycations using layer-by-layer self-assembly was recently reported.[26] The driving force for this research is the expectation of fast computational systems through the miniaturization of microelectronic circuit components to the nanoscale.[27−30] The study of structure/property relationships in wirelike molecules is a key topic for current investigations, and the use of the molecular structure in electronic circuits is usually achieved via terminal thiol-gold contacts.[31] The efficiency of electronic communication is based on the use of molecules that possess delocalized π-systems with low HOMO−LUMO gaps. Rigid-rod π-conjugated oligomers and model molecules constitute a potentially new class of molecular wires.[32] There have been several studies of electron transfer involving such materials with thiol, α,ω-dithiol, thioacetyl, or α,ω-dithioacetyl end groups,[33,34] which are necessary for the formation of self-assembled monolayers or covalent connections between proximate gold electrodes.[35,36]

† Part of the "Vincenzo Aquilanti Festschrift".

* Corresponding author. Phone: (+) 39-06-57333388. Fax: (+) 39-06-57333390. E-mail: battocchio@fis.uniroma3.it.

† University of Rome "La Sapienza".

‡ University of Napoli "Federico II".

§ University of Rome "Roma Tre".

10.1021/jp904865k
Published on Web 08/12/2009

SCHEME 1: Chemical Structures of Pd(II) Chlorides, Thioacetate Complexes, Free and Gold Anchored Thiols

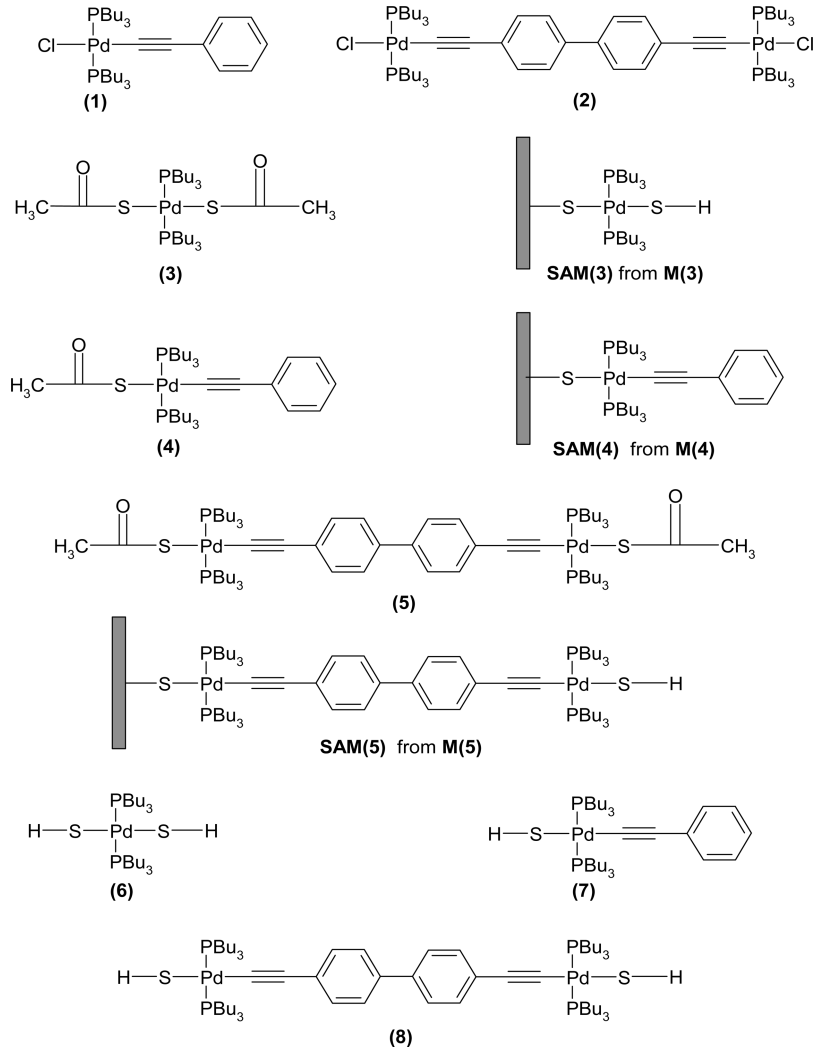

In this framework, we have devoted our research to the synthesis and characterization of mono and bimetallic palladium complexes in which the metal atom is σ-bound to sulfur-containing ligands. In this paper, we describe the preparation and characterization of SAMs based on Pd(II) organometallic complexes grown onto a Au/Si(111) surface, whose structure is shown in Scheme 1. The use of organometallic thiol complexes as stabilizing agents for gold surfaces or nanoclusters offers a promising perspective for the applications of these materials,[37,38] and in-depth investigation of the molecular structures of organometallic SAMs is an important goal for defining their self-assembling behavior and properties. High-resolution X-ray photoelectron spectroscopy (HR-XPS) is a very well suited technique to investigate the molecule−substrate interaction in SAMs because the high spectral resolution and photon flux allow one to ascertain the identity of the headgroup−substrate interface. HR-XPS measurements combined with near edge X-ray absorption fine structure (NEXAFS) and reflection absorption infrared spectra (IRRAS) studies were carried out to achieve a structural and electronic characterization of the organometallic SAMs.

2. Experimental Section

FTIR spectra in the range 400−4000 cm^{-1} were recorded with a Bruker Vertex 70 Fourier transform spectrometer as film deposited from CH_2Cl_2 solutions on ZSM5 CsI cells. ^1H, ^{13}C, and ^{31}P NMR spectra were recorded on a Varian 300 spectrometer at 300, 75, and 121 MHz, respectively. ^1H and ^{13}C chemical shifts (parts per million) are reported in δ values relative to internal standard $(CH_3)_4Si$; $CDCl_3$ (δ 7.24) and C_6D_6 (δ 7.15) were used as solvents for ^1H NMR spectra as well as for ^{13}C NMR spectra ($CDCl_3$ δ 77.0; C_6D_6 δ 128.0 ppm). The ^{31}P chemical shifts are relative to a H_3PO_4 (85%) probe. UV−vis spectra were recorded by a Varian-Cary 100 spectrophotometer. Photoluminescence (PL) spectra were registered on a Perkin-Elmer LS 50 spectrofluorometer. UV and PL measurements were performed at room temperature using CH_2Cl_2 quantitative solutions of the compounds in quartz cells. The molar extinction coefficient, $\varepsilon°$, and the relative quantum yield, η, of CH_2Cl_2 solutions of the complexes were also determined as reported in the literature.[39] Elemental analyses were provided by the Servizio di Microanalisi of the Department of Chemistry, on an EA 1110 CHNS-O instrument.

XPS spectra were obtained using a custom-designed spectrometer. A non-monochromatized Mg Kα X-ray source (1253.6 eV) was used, and the pressure in the instrument was maintained at 1×10^{-9} Torr throughout the analysis. The experimental apparatus consists of an analysis chamber and a preparation chamber separated by a gate valve. An electrostatic hemispherical analyzer (radius 150 mm) operating in the fixed analyzer transmission mode and a 16-channel detector giving a total instrumental resolution of 1.0 eV as measured at the Ag $3d_{5/2}$

core level were used. The film samples were prepared by dissolving our materials in $CHCl_3$ and spinning the solutions onto polished stainless steel substrates. The samples showed good stability during the XPS analysis, preserving the same spectral features and chemical composition. The spectra were energy-referenced to the C1s signal of aliphatic C atoms, having a binding energy of BE = 285.00 eV, in those samples containing mainly aliphatic carbons, to the C 1s signal of BE = 284.7 eV in those containing more aromatic carbon atoms, in agreement with literature data.[40] Curve-fitting analysis of the C 1s, Pd 3d, P 2p, S 2p, and O 1s spectra was performed using Gaussian curves as fitting functions (typical full width at half-maximum, fwhm, in the range 1.7−2.1 eV) after subtraction of a Shirley-type background. Quantitative evaluation of the atomic ratios was obtained by analysis of the XPS signal intensity employing Scofield's atomic cross-section values and experimentally determined sensitivity factors.[41]

Data collections for X-ray diffraction (XRD) crystal structure determination were performed in flowing N_2 at 173 K for **2** and at room temperature for **5** and **7** on a Bruker-Nonius kappa CCD diffractometer (Mo Kα radiation, CCD rotation images, thick slices, φ scans + ω scans to fill the asymmetric unit). Cell parameters were determined from 266 reflections in the range $4.31° \leq \theta \leq 18.816°$, 99 reflections in the range $3.86° \leq \theta \leq 21.45°$, and 16 reflections in the range $3.62° \leq \theta \leq 14.87°$ for **2**, **5**, and **7**, respectively. Semiempirical absorption corrections (multiscan SADABS)[42] were applied. All structures were solved by direct methods (SIR 97 package)[43] and refined by the full matrix least-squares method (SHELXL program of the SHELX97 package)[44] on F2 against all independent measured reflections using anisotropic thermal parameters for all non-hydrogen atoms. H atoms were placed in calculated positions with Ueq equal to those of the carrier atom and refined by the riding method. Evidence of high thermal motion and positional disorder was found for the butyl groups in **2** and **7**.

HR-XPS measurements were performed at the synchrotron storage ring ELETTRA using the BACH (*b*eamline for *a*dvanced di*ch*roism) beamline and relative experimental station that is connected to an undulator front end. To probe the S 2p and Au 4f core levels, an excitation energy of 699 eV was used, a photon energy value leading to the optimization of the photoelectron yield for both core levels. The spectra were acquired in normal emission geometry, and the resolution was better than 0.1 eV. The S 2p binding energy for every sample was individually calibrated using th eAu $4f_{7/2}$ photoemission line at 83.95 eV[45] of the thiol-covered Au substrate. The spectra were fitted by Gaussian functions, and a Shirley background was previously subtracted.[46] The S $2p_{3/2}$, S $2p_{1/2}$ spin−orbit doublet was fitted by using the same full width at half-maximum (fwhm) value for both components, a spin−orbit splitting of 1.20 eV, and an intensity ratio S $2p_{3/2}$/S $2p_{1/2}$ of 2/1. When several different species were found in the same spectrum, the same fwhm value was used for all individual peaks.

Angular dependent synchrotron-induced NEXAFS experiments were performed at the ELETTRA storage ring at the bending magnet for emission absorption and reflectivity beamline, installed at the left exit of the 8.1 bending magnet exit. The apparatus is based on a bending magnet as a source, beamline optics delivering photons from 5 up to about 1600 eV with a selectable degree of ellipticity. The UHV end station has a movable hemispherical electron analyzer and a set of photodiodes to collect angle-resolved photoemission spectra, optical reflectivity, and fluorescence yield. To examine the molecular orientation, the incident angle of the linearly polarized synchrotron radiation was varied from normal (90°) to grazing (20°) incidence with respect to the sample surface. The photon energy and resolution were calibrated and experimentally tested at the K absorption edges of Ar, N_2, and Ne. In addition, our carbon K-edge spectra have been further calibrated using the resonance at 285.50 eV assigned to the C 1s-π^* ring transition. The raw C K-edge NEXAFS spectra were normalized to the incident photon flux by dividing the sample spectrum by the spectrum collected on a freshly sputtered gold surface. The spectra were then normalized, subtracting a straight line that fits the part of the spectrum below the edge and assessing to 1 the value at 320.00 eV. IRRAS measurements were carried out on a Bruker Vertex 40 instrument equipped with a grazing incidence reflection unit (Bruker). Incidence light was reflected from the samples at angles of incidence 0° and 90°. The final spectra were averaged from 64 scans at a spectral resolution of 4 cm^{-1}.

2.1. Materials. All reactions were performed under inert argon atmosphere. Solvents (Carlo Erba) were dried on Na_2SO_4 and subjected to argon bubbling before use. All chemicals, unless otherwise stated, were obtained from commercial sources and used as received. The precursor palladium complex, *trans*-$[Pd(PBu_3)_2Cl_2]$, was prepared according to literature methods.[47] 4,4′-Diethynylbiphenyl, DEBP, was obtained starting from the silyl derivative, 4,4′-trimethylsilyldiethynylbiphenyl, DEBP-Si, following a reported procedure.[48] Phenylacetylene was purchased from Aldrich and distilled before use. Potassium thioacetate and sodium hydrosulfide hydrate were purchased from Aldrich and were used without further purifications. Preparative thin-layer chromatography separation was performed on 0.7 mm silica plates (Merck Kieselgel 60 GF254), and chromatographic separations were obtained with 70−230 mesh silica (Merck) and proper solvents as the eluant.

2.2. Syntheses. The full synthesis methodology and characterization of precursor complexes *trans*-$[(C_6H_5-C\equiv C)Pd(PBu_3)_2Cl]$ (**1**) and *trans*,*trans*-$[Cl(PBu_3)_2Pd(C\equiv C-C_6H_4-C_6H_4-C\equiv C)Pd(PBu_3)_2Cl]$ (**2**), of thiolates *trans*-$[Pd(PBu_3)_2(SCOCH_3)_2]$ (**3**) and *trans*-$[(C_6H_5C\equiv C)Pd(PBu_3)_2(SCOCH_3)]$ (**4**), and of thiols *trans*-$[Pd(PBu_3)_2(SH)_2]$ (**6**) and *trans*-$[(C_6H_5C\equiv C)Pd(PBu_3)_2(SH)]$ (**7**) are reported in the Supporting Information. The synthesis and characterization of the complexes *trans*,*trans*-$[(CH_3COS)Pd(PBu_3)_2(C\equiv C-C_6H_4-C6H4-C\equiv C)(PBu_3)_2Pd(SCOCH_3)]$ (**5**) and *trans*,*trans*-$[(HS)Pd(PBu_3)_2(C\equiv C-C_6H_4-C_6H_4-C\equiv C)(PBu_3)_2Pd(SH)]$ (**8**) are here described as representative examples.

Trans,trans-[(CH₃COS)Pd(PBu₃)₂(C′C−C₆H₄−C6H4−C′C)(PBu₃)₂Pd(SCOCH₃)] (5). Compound *trans*,*trans*-$[Cl(PBu_3)_2Pd(C\equiv C-C_6H_4-C_6H_4-C\equiv C)Pd(PBu_3)_2Cl]$ (**2**), (0.100 g, 0.08 mmol) was dissolved in 50 mL of CH_2Cl_2, and 0.019 g (0.17 mmol) of $KSCOCH_3$ was added. The solution was stirred at room temperature for 4 days, then filtered, and the solvent was removed. The crude product (**5**) was an orange-brown solid that was crystallized from CH_2Cl_2/CH_3OH at 4 °C. Pale-yellow single crystals were obtained. Yield: 95%. Melting point: 62−63 °C. Anal. calcd: C 59.53 (59.50), H 9.11 (8.96), S 5.04 (4.67). FTIR (film, cm^{-1}): 2108 (ν C≡C), 1623 (ν C═O), 1261 (ν S−C═O). UV (CH_2Cl_2, nm): $\lambda_{max} = 332$; $\varepsilon° = 64.78$ (10^3 L mol cm^{-1}). Luminescence emission (CH_2Cl_2, nm): $\lambda_{max} = 450$; $\eta = 0.8\%$. NMR ($CDCl_3$, δ ppm): ^{1}H, 0.92 (t, $J = 7.2$ Hz, CH_3), 1.44 (m, CH_2), 1.55 (m, CH_2), 1.94 (m, P−CH_2), 2.36 (s, CH_3−C═O), 7.30 (d, Ar−H), 7.45 (d, Ar−H); ^{13}C, 13.74 (s, CH_3), 24.39 (t, JC-*P* = 6.7 Hz, CH_2), 23.49 (t, JC-*P* = 13.7 Hz, P-CH_2), 26.45 (s, CH_2), 35.03 (s, CH_3−C═O), 106.21 (t, JC-*P* = 17.3 Hz, C≡C), 107.54 (t, JC-*P* = 4.5 Hz, C≡C),

126.25 (s, Ar−C), 126.91 (s, Ar−C), 130.81 (s, Ar−C), 137.58 (s, Ar−C), 205.25 (s, C═O); ^{31}P ($CDCl_3$, δ ppm): 10.40 (s).

Trans,trans-[(HS)Pd(PBu$_3$)$_2$(C≡C−C$_6$H$_4$−C$_6$H$_4$−C′C)-(PBu$_3$)$_2$Pd(SH)] (8). Compound *trans*,*trans*-[Cl(PBu$_3$)$_2$Pd-(C≡C−C$_6$H$_4$−C$_6$H$_4$−C≡C)Pd(PBu$_3$)$_2$Cl] (**2**) (0.10 g, 0.08 mmol) was dissolved in 20 mL of THF, and 0.037 g (0.66 mmol) of NaSH was added. The solution was stirred at room temperature for 2 days, and the subsequent work-up followed the same procedure reported in compound **6**. The pure product is a yellow, waxy solid. Yield: 87%. Melting point: 90 °C. Elem. anal. % (calcd %): C 60.04 (59.66); H 9.36 (9.23); S 5.35 (4.98). FTIR (film, cm^{-1}): 2108 (ν C≡C); 1603 (ν C═C); 2570 (ν S−H). UV (CH_2Cl_2, nm): λ_{max} = 322; $\varepsilon°$ = 64.48 (10^3 L mol cm^{-1}). Luminescence emission (CH_2Cl_2, nm): λ_{max} = 354, η = 0.84%. NMR ($CDCl_3$, δ ppm): ^{1}H, 0.93 (t, J = 7.0, CH_3), 1.45 (m, CH_2), 1.57 (m, CH_2), 1.95 (m, P−CH_2), 13.32 (t, J = 11.4 Hz, S−H), 7.30 (d, Ar−H), 7.46 (d, Ar−H); ^{13}C, 13.78(s, CH_3), 26.56 (s, CH_2), 24.38 (t, J_{C-P} = 6.6 Hz, CH_2), 23.53 (t, J_{C-P} = 13.9 Hz, P−CH_2), 105.45 (t, J_{C-P} = 4.5 Hz, C≡C), 109.04 (t, J = 17.7 Hz, C≡C), 132.53 (s, Ar−C), 130.99 (s, Ar−C), 128.00 (s, Ar−C), 126.58 (s, Ar−C); ^{31}P ($CDCl_3$, δ ppm): 9.99 (s).

2.3. Multilayers and SAMs Preparation. For the preparation of multilayers and self-assembled monolayers, terminal thiol compounds were in situ obtained by a deacylation procedure carried out on precursor thiolate complexes **3**, **4**, and **5**, and allowed to self-assemble on gold surfaces. Gold-coated silica wafers prepared by growing a Au film 4000 Å thick onto Si(111) substrates were cut into slides (ca. 1 cm^2) and washed with several organic solvents—acetone, ethanol, chloroform—and blown dry with nitrogen. The substrates were then dipped into the proper, just obtained thiol solution to achieve the anchoring.

Preparation and anchoring of multilayer **M(3)**: compound **3** (0.040 g, 0.06 mmol) was dissolved in 20 mL of THF, and 260 μL of NH_4OH (30%) was added.

Preparation and anchoring of multilayer **M(4)**: compound **4** (0.030 g, 0.04 mmol) was dissolved in 25 mL of THF, and 110 μL of NH_4OH was added.

Preparation and anchoring of multilayer **M(5)**: compound **5** (0.035 g, 0.02 mmol) was dissolved in 15 mL of THF, and 125 μL of NH_4OH was added.

The solutions were stirred at 30 °C for 2 h and filtered on Celite, and freshly washed gold substrates were dipped into the solution for 4 h. The multilayers **M(3)**, **M(4)**, and **M(5)** were rinsed with different solvents (ethanol, THF, and acetone) to achieve the formation of **SAM(3)**, **SAM(4)**, and **SAM(5)** films in the monolayer thickness regime.

3. Results and Discussion

3.1. Preparation and Characterization of Organometallic Palladium Complexes. *trans*-[Pd(PBu$_3$)$_2$Cl$_2$] reacted with phenylacetylene or 4,4′-diethynylbiphenyl to give mononuclear and binuclear complexes **1** and **2**, respectively, and these compounds were used as starting materials for the preparation of thioacetate complexes **3**, **4**, and **5**, suitable for the self-assembling procedure on gold surfaces. In our study, the deacylation of thioacetyl groups to achieve terminal thiols was carried out in situ by using the weak base NH_4OH, and a series of well-defined, easily handled, functionalized multilayers **M(3)**, **M(4)**, and **M(5)** were prepared through the direct anchoring onto gold surfaces. For comparison, terminal thiols **6**, **7**, and **8** were also prepared and isolated in high yields by ligand exchange reaction from Pd(II) chlorides in the presence of NaSH (see the Experimental Section). The chemical structures of palladium chlorides, thioacetates, and thiols anchored on gold are depicted in Scheme 1.

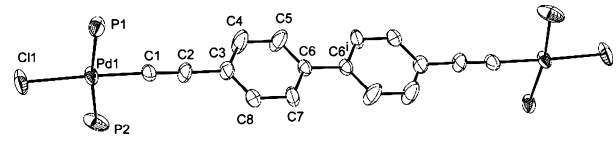

Figure 1. ORTEP view of **2**. Thermal ellipsoids are shown at 30% probability level. Butylic tails of PBu_3 and all hydrogen atoms are not shown for clarity. $i = -x + 1, -y - 1, -z + 1$.

Metal−carbon coupling between a Pd(II) dichloride complex and terminal alkynes has been applied for the preparation of complexes **1** and **2** with relatively high yields, following a dehydrohalogenation general synthetic pathway.[49] To avoid the isolation of the oxidatively unstable free thiol complexes, potassium thioacetate was selected as the nuclophile for displacing the chloride ligands. The target compounds **3**, **4**, and **5** were synthesized by a typical metal-halide-exchange reaction according to a procedure similar to that described for Pd(II) complexes by different groups.[50−57]

The FTIR spectra of the Pd(II) acetylyde complexes **1**, **2**, **4**, **5**, **7**, and **8** showed a single signal of the C≡C stretching mode around 2100 cm^{-1}, and the presence of the thioacetyl ligand was assessed by the sharp signal at around 1626 cm^{-1} (νC═O) and 946 cm^{-1} (νC−S) in compounds **3**, **4**, and **5**. Such absorption bands evidence a unidentate coordination of thioacetyl via the sulfur atom to palladium and indicate the absence of significant palladium−oxygen interactions,[58] confirmed by the crystal structure (see, for example, Figure 1). The IR spectra of thiol-containing compounds **6**, **7**, and **8** showed a weak signal at about 2500 cm^{-1}, consistent with the S−H stretching mode.[59,60]

^{1}H NMR spectra of the compounds exhibited the typical pattern of the phosphine resonances at about 0.9, 1.4, 1.6, and 1.9 ppm and a double doublet typical pattern of the biphenyl or phenyl ligand at 7.29 and 7.45 ppm. A single signal at around 2.36 ppm was detected for compounds **3**, **4**, and **5**, confirming the presence of the thioacetyl ligand. The signal at about 13.3 ppm in compounds **6**, **7**, and **8** confirmed the presence of S−H terminal thiol ligands.

The ^{13}C NMR spectra show the expected resonances of phosphine ligands, diethynylbiphenyl moiety, and of ending phenyl ligands for all the examined complexes. In addition, a single signal at about 205 ppm due to the carbonyl carbon appeared in the spectra of thioacetate complexes **3**, **4**, and **5**.

Single resonances in the ^{31}P NMR spectra were observed for all compounds at about 10.44 ppm for chlorides, in the range 9.43−10.40 ppm for thioacetates, and in the range 8.45−9.99 ppm for thiol Pd(II)-based complexes.

XRD measurements highlight the molecular structure of **2**, reported in Figure 1. The asymmetric unit contains a half molecule of the dimer, laying the molecule on an inversion center located at the midpoint of the central C−C bond of the biphenyl group, showing analogies with related compounds.[61] The coordination environment of the palladium atom is square-planar (angles are in the range 84.6−94.4°), with two trans PBu_3 groups and trans chloride and acetylide moieties. As already noted in the literature,[62] a slight deformation in the coordination of the metal atom is observed, probably due to a repulsive interaction between the chloride atom and the phosphine ligands. The Pd−C and C≡C bond lengths of 1.934(12) and 1.213(15) Å, respectively, are typical for metal−σ-acetylide moieties.

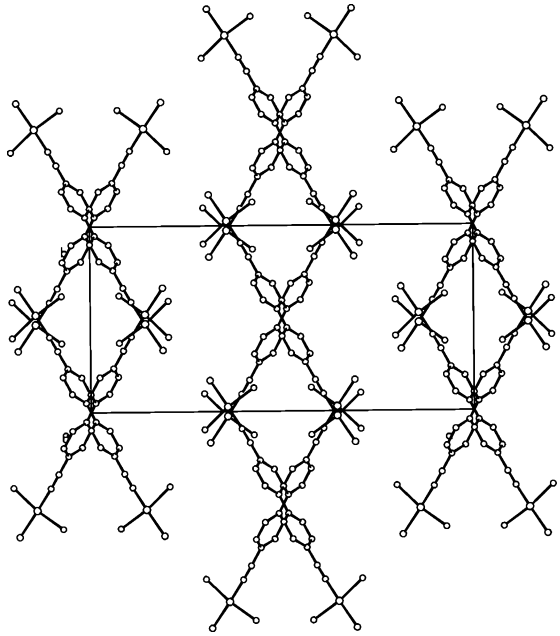

Figure 2. Crystal packing of **2**, view along [001] direction.

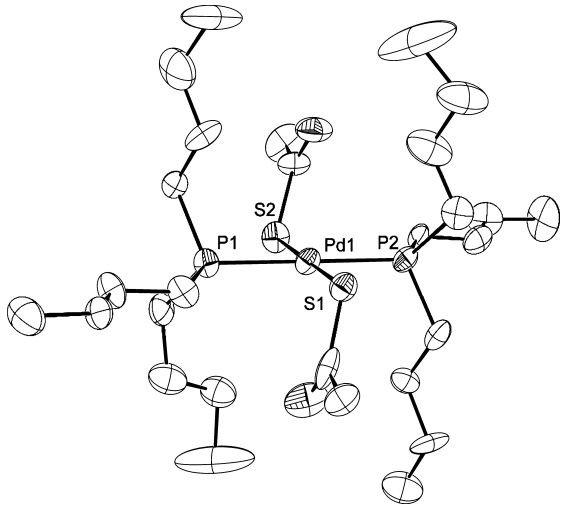

Figure 3. ORTEP view of **3**. Thermal ellipsoids are shown at 30% probability level. All the hydrogen atoms are not shown for clarity.

A partial conjugation can be observed, being C1≡C2 and C2−C3 bond lengths, respectively longer and shorter (1.213(15) and 1.474(13) Å) compared to typical nonconjugated bonds. The position of the halogen atom and of the acetylide moieties is almost linear (Cl−Pd−C = 177.7(4)°, Pd−C≡C = 177.3(1)°), confirming the linearity of the whole molecule and, then, the rigid rod nature of this model compound. The biphenyl moiety, lying on the inversion center, is strictly planar, and its mean plane is quite perpendicular to the coordination plane of the metal [angle between their mean planes is 82.0(3)°]. The complex **2** is essentially isostructural with the analogous Pt(II) complex, recently described.[63] No significant differences were found in the coordination environment or in the geometric parameters, in line with the similarity of the palladium and platinum covalent radii.[64] The crystal packing of **2** shows two separate sets of molecules piled along c, tilted relative to each other at about 70° (Figure 2).

The molecular structures of **3** and **5** obtained from X-ray diffraction studies, are reported in Figures 3 and 4. It is worth noting that in both complexes, the thioacetate groups coordinate

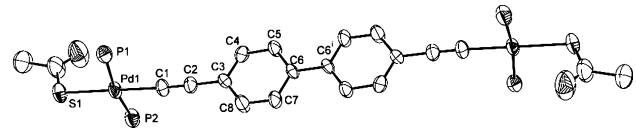

Figure 4. ORTEP view of **5**. Thermal ellipsoids are shown at 30% probability level. Butylic tails of PBu3 and all hydrogen atoms are not shown for clarity. $i = -x + 1, -y, -z + 1$.

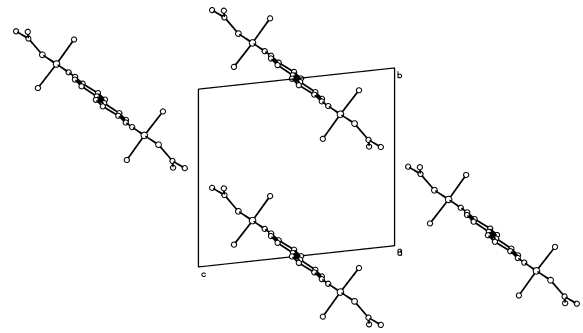

Figure 5. Crystal packing of **5**, view along [100] direction.

the metal through the S atoms. In the mononuclear complex **3**, a square-planar environment around the metal with two *trans*-PBu_3 and two thioacetate groups is present (angles are in the range 86.4−93.4°). The two pendant oxygen atoms of the thioacetate groups show the sterically more favorable anti conformation, as observed for the analogous Pd(II) complex *trans*-[Pd(kS-S{O}CMe)$_2$(PPh$_3$)$_2$].[46] The Pd−P [2.308(4) and 2.330(4) Å] and Pd−S [2.300(4) and 2.346(4) Å] bond lengths fall in the range found for the above-mentioned compound and are also consistent with the literature data.[65]

The molecular structure of **5** presents significant geometrical similarities to **2**. The molecule sits on a crystallographic center of symmetry located at the midpoint of the C−C bond of the biphenyl group, which is perfectly planar. The square planar coordination geometry presents two trans PBu_3 groups and the thioacetate ligand with the acetylide moiety trans to each other. As expected, the molecule is linear and shows an inclination of 83.5(3)° between the mean planes of the biphenyl moiety and the metal coordination plane. All the bond distances and angles are in agreement with those of complex **2**. The only relevant difference is a lengthening of the Pd−C1 bond distance trans to the thioacetate group with respect to Pd−C1 trans to chloride (2.01(1) Å to compare with 1.93(1) Å), probably attributable to the major trans influence of the sulfur ligand with respect to the chloride. The crystal packing of **5** presents two separate domains, one containing the aliphatic moieties and the other the aromatic ones. The molecules dispose in parallel layers, piled along $-b + c$ (Figure 5.).

UV−vis absorption and emission spectra of the organometallic molecules have been recorded to investigate the structure/properties relationship. The absorption maxima showed peaks in the range 270−330 nm. Comparing the UV spectra of the Pd(II) acetylyde complexes with those of the corresponding organic precursors, that is, phenylacetylene (λ_{max} = 246 nm) and DEBP (λ_{max} = 290 nm), a red shift of the UV absorption was generally observed due to higher π delocalization. The UV spectrum of complex **2** shows two absorption maxima at 275 and 328 nm; the latter one, the most intense, is due to the $\pi \rightarrow \pi^*$ transitions, and the first one, weaker, is due to atomic orbital $d-d$ transitions of the metal. The emission properties of Pd(II) compounds were also investigated and showed emission maxima in the range 300−450 nm with luminescence quantum yield

values between 0.10 and 3.8%, the latter being worthy of notice for organometallic molecules.

To better assess the complexes' electronic structures, a low-resolution X-ray photoelectron spectroscopy (XPS) investigation was performed. C 1s, P 2p, Pd 3d, Cl 2p, and S 2p core level spectra were collected, and the measured binding energy (BE) values appeared consistent with those already published for Pd-containing polymetallaynes[35] and expected for the proposed molecular structures (confirmed by XRD results). The core level BE values (reported in the Supporting Information) are quite close for samples bearing the same tail group, showing that the configuration and electronic structure of the metal center is not affected by the substitution of the terminal ligand (Cl, SH, or $SCOCH_3$), thus confirming that the overall molecular geometry, that is, a square planar arrangement of the ligands around the transition metal, is preserved in all samples.

In detail, the Cl 2p BE value for samples **1** and **2** was found at 197.62 eV, which is the same as reported for similar Pd complexes.[66] The Pd 3d spectra collected for all the samples here considered were also analyzed by curve fitting, and appeared structured with two pairs of spin orbit components. The main Pd $3d_{5/2}$ component found occurring at about 337.6 eV BE was attributed to Pd(II) tetracoordinated by comparison with the Pd $3d_{5/2}$ signal of the pristine square planar Pd complex (the Pd $3d_{5/2}$ peak in *trans*-$[Pd(PBu_3)_2Cl_2]$ has been recently found at BE = 338.1 eV). The observed decrease in the Pd 3d BE of samples **1** and **2** with respect to the precursor complex reflects an increase in charge density at the Pd sites and has been ascribed to the presence of additional coordination of acetylenic groups by the Pd atoms; in our case, belonging to the DEBP moiety of a neighboring molecule in an intermolecular assembling, as also suggested by literature data. The presence of a negligible amount of Pd(0) was detected by the occurrence of a minor $3d_{5/2}$ contribution at lower BE values (336.1 eV). For samples **1** and **2**, Cl/Pd intensity ratios equal to 1/1 were estimated. The P 2p spectra of all samples show peaks at about 130.8 eV BE, in agreement with the values reported in the literature for metal-bonded phosphine groups,[67] and the Pd/P atomic ratio is 1/2 for all the samples, as expected. For thiolate and thiol ending group-containing compounds, the S 2p core spectra appeared structured by two spin−orbit components. The spectra have been analyzed by curve-fitting, obtaining the expected BE separation of 1.20 eV as well as an atomic ratio of 2/1 (S $2p_{3/2}$−S $2p_{1/2}$). The S $2p_{3/2}$ spin−orbit component for thiolate samples **3**, **4**, and **5** was observed at 162.0 eV, a BE value fully consistent with those reported in the literature for sulfur-containing molecules interacting with metals through the formation of a sulfur−metal chemical bond.[68] The S/Pd atomic ratios were estimated for all mononuclear and binuclear samples. For complexes and thiol samples **6**, **7**, and **8**, a value of about 1/1 was found, as expected from the proposed molecular structure. For sample **5**, a S/Pd value of about 2/1 was calculated, which is in excellent agreement with the chemical structure reported in Scheme 1. XPS results support the chemical structure assessments obtained from the other characterizations and from the XRD crystal structure analysis and confirm the stability of the thiolate and thiol complexes toward X-ray exposition.

3.2. Multilayers and SAMs Achievement and Characterization. To establish the potentiality of these molecules as candidates in electrical circuits, we have investigated their self-assembly on gold-coated substrates and performed preliminary experiments on the resulting multi- and monolayer films. The low concentrations (typically 1−2 mM) of the solutions of complexes that are used in the preparation of SAMs allowed us to use different solvents. In our case, a THF solution of thiolate precursors was used. Thiol substituents can directly form self-assembled multilayers and monolayers on gold surfaces;[69] however, because of the oxidative instability of organometallic thiol groups, the thioacetyl protecting functionality was introduced, and thiols were produced in situ by a deacylation reaction. In situ monitoring by FTIR and UV techniques of the deacylated thiol complex solutions was compared with the solutions of on-purpose prepared terminal thiols **6**, **7**, and **8**, thus confirming the achievement of the terminal thiol functionality. The solution was allowed to react, then freshly cleaned gold substrates were introduced. Self-assembled monolayers are formed very rapidly on the substrate; however, it was necessary to use adsorption times of 15 h or more to get multilayers **M(3)**, **M(4)**, and **M(5)**.

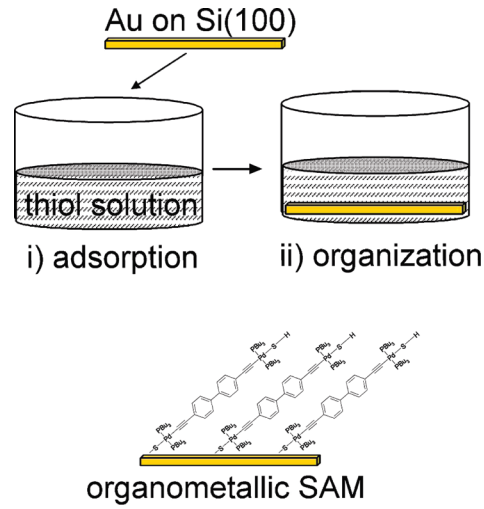

Figure 6. SAM preparation.

Neat **SAM(3)**, **SAM(4)**, and **SAM(5)** were obtained by rinsing the substrates with different organic solvents. A schematic outline of the SAM preparation procedure on gold substrates is given in Figure 6.

To perform a preliminary evaluation of the coverage and molecular orientation of the so-far-obtained multilayer samples, IRRAS spectra were collected. The Au−S bond is strong and contributes to the stability of the multilayers together with the van der Waals forces between adjacent methylene groups. The CH stretching vibrations of the alkyl chains are very sensitive to packing density and to the presence of gauche defects, which makes them ideally suited as probes to determine the quality of the films.[70] Our choice was to compare samples with a different number of metallic centers (i.e. **M(3)** and **M(5)**) and to study the behavior of the methylenic chains of PBu_3 ligands. In particular, the antisymmetric CH_2 stretching vibration is a useful indicator; comparing **M(3)** and **M(5)**, a variation from 2926 to 2930 cm^{-1} was observed, together with a broadening of the peak. A variation in the symmetric CH_2 stretching vibration was also observed, and **M(3)** and **M(5)** showed peaks at 2960 and 2957 cm^{-1}, respectively. These differences are indicative of a lower-order degree of in the **M(5)**, probably due to a higher steric hindrance induced by the organic spacer and from the presence of two metallic centers.

3.2.1. High-Resolution X-ray Photoelectron Spectroscopy. As for the organometallic thiols discussed in this work, since these materials are new, the acquiring of reliable information on both molecular structures and properties of the SAMs formed from these samples is a mandatory task for defining their self-assembling behavior. HRXPS is very well suited to investigating

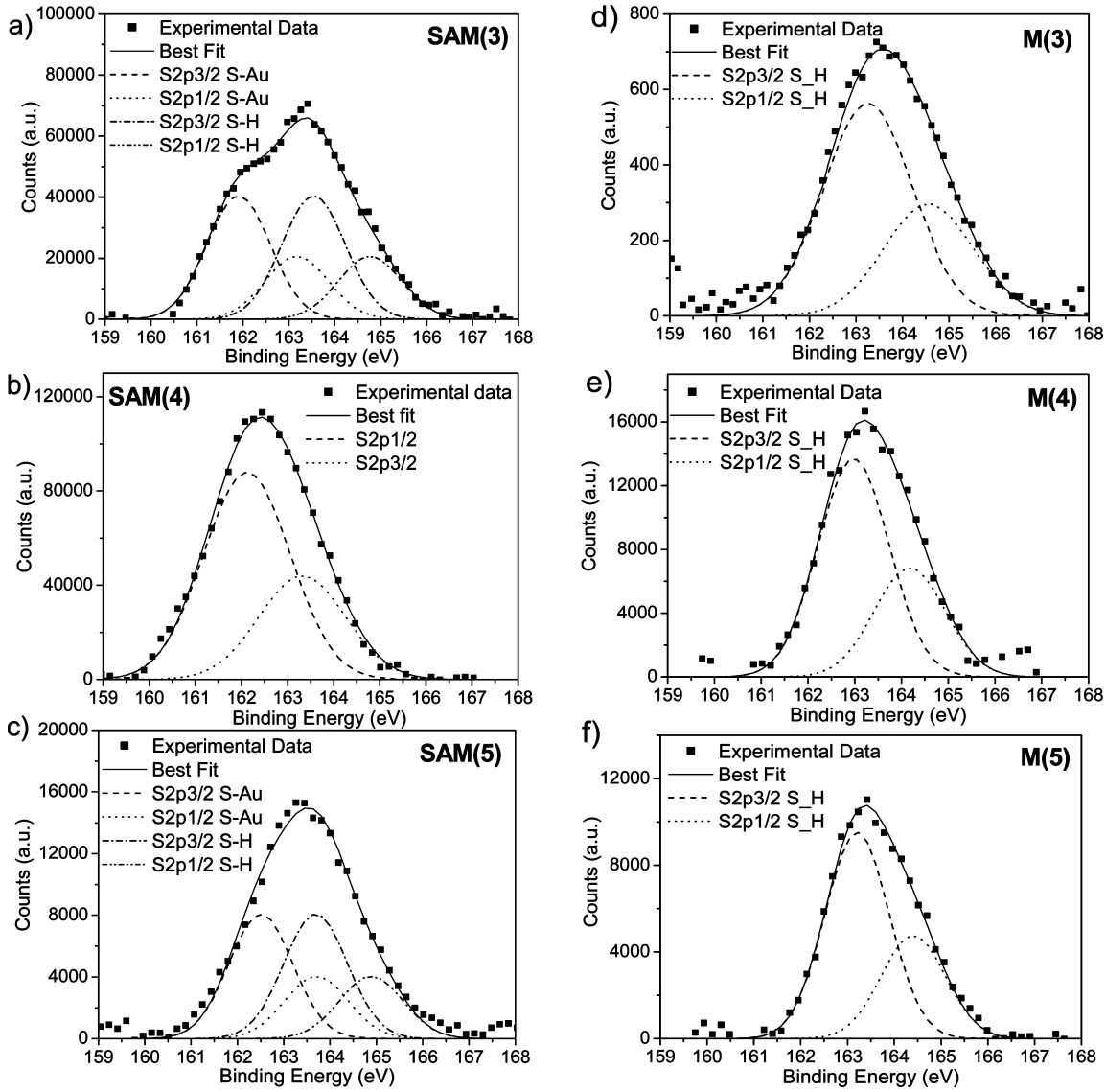

Figure 7. (a, b, c) S 2p HRXPS spectra of monolayers **SAM(3)**, **SAM(4)**, and **SAM(5)**; (d, e, f) S 2p HRXPS spectra of **M(3)**, **M(4)**, and **M(5)**.

the molecule−substrate interaction in SAMs because the high spectral resolution and photon flux allow one to establish the chemistry occurring at the headgroup−substrate interface.

To ascertain that the SAM systems were efficiently obtained by following the procedure described above and to investigate the molecule−substrate interaction, high resolution XPS spectra were collected for Au4f and S2p core levels. S 2p HRXPS spectra of **SAM(3)**, **SAM(4)**, and **SAM(5)** are shown in Figure 7a, b, and c; the same spectra collected on **M(3)**, **M(4)**, and **M(5)** are reported in Figure 7d, e, and f. The peak position, fwhm, and relative intensities are reported in Table 1.

As expected, all the S 2p spectra show a spin−orbit doublet (S $2p_{1/2}$, S $2p_{3/2}$); the more intense S $2p_{3/2}$ component is taken as reference and reported in the table. The BE position of this signal indicates whether the sulfur atom is covalently bonded to the metal surface or it is not. For thiolate species chemisorbed on metals, an S $2p_{3/2}$ BE value of nearly 162 eV is expected;[67] S $2p_{3/2}$ signals around 163.5 eV are usually assigned to physisorbed molecules at the SAM−ambient interface[71] or physisorbed thiols.[72,29] For the SAM systems obtained from sample **3**, **SAM(3)**, two S 2p spin−orbit doublets are observed with the $2p_{3/2}$ component occurring at 162.0 eV and 163,7 eV.

TABLE 1: HR-XPS Data for Multi- and Monolayers: M(3), M(4), M(5), SAM(3), SAM(4) and SAM(5) on Gold

sample/signal	BE (eV)	fwhm (eV)	atomic ratios (S a/S b)	est. thickness (nm)
SAM(3)				0.2
S $2p_{3/2}$ S-Au (S a)	162.0	1.58	1	
S $2p_{3/2}$ SH (S b)	163.7	1.58	1	
M(3)				
S $2p_{3/2}$ SH (S b)	163.2	1.83	1	
SAM(4)				0.4
S $2p_{3/2}$ S−Au (S a)	162.1	1.70		
M(4)				
S $2p_{3/2}$ SH (S b)	163.0	1.90		
SAM(5)				1.1
S $2p_{3/2}$ S−Au (S a)	162.5	1.61	1	
S $2p_{3/2}$ SH (S b)	163.6	1.61	1	
M(5)				
S $2p_{3/2}$ SH (S b)	163.2	1.61		

The low-energy S $2p_{3/2}$ peak (S a) is ascribed to sulfur bonded to gold, subsequent to the anchoring of the thiol on the metal surface, whereas the high-energy S $2p_{3/2}$ signal (S b) is assigned to sulfur in the free thiol terminal group. Since the relative contributions of the different sulfur-containing species can be

estimated from the ratio between the respective signal intensities (peak areas), the calculated intensity ratio S a/S b = 1/1 indicates that 50% of the S-terminal groups in **SAM(3)** are covalently bonded to the gold surface, and therefore, only one of the two thiol-ending groups appears to be involved in the interaction. The molecular structure (see Scheme 1) of **SAM(3)** suggests that for steric effects due to the tributylphosphine groups array, the molecules should graft the substrate surface with one sulfur atom, whereas the second −SH group should remain free. The above hypothesized molecular arrangement is fully supported by the HRXPS S 2p spectra, reported in Figure 7a. In Figure 7d, the S 2p signal collected for sample **3** prior to rinsing (thick layer **M(3)**) is also displayed. The multilayer spectrum shows a pair of spin orbit components only, with an S $2p_{3/2}$ BE of 163.2 eV, a value consistent with physisorbed thiol molecules and, therefore, two equivalent −SH groups, as expected for a thick film.

Similar to **SAM(3)** and **M(3)**, the S 2p spectrum for samples **SAM(5)** (Figure 7c) and **M(5)** (Figure 7f) presents two pairs of spin orbit components for the monolayer film and one pair for the multilayer system. The S $2p_{3/2}$ BE values observed for this sample are fully consistent with those already discussed for **SAM(3)** and **M(3)**, as shown in Table XPS. As for the atomic ratios in the monolayer sample, an S a/ S b ratio value of 1/1 was estimated. Assuming that the peak at 163.6 eV originates from free thiol terminal groups, the observed intensity ratio suggests that as for **SAM(3)**, in the **SAM(5)** sample, the molecules graft the gold surface with only one terminal group.

HRXPS spectra of monolayer and multilayer systems obtained by grafting on gold sample **4** are also reported (Figure 7b and e, respectively). For this sample, a single pair of spin−orbit components is observed in both monolayer and multilayer regimes. The S $2p_{3/2}$ signal for **SAM(4)** in the monolayer regime occurring at about 162 eV indicates that all molecules are covalently bonded to the gold surface. Conversely, the S $2p_{3/2}$ BE value of 164 eV observed for **M(4)** suggests, as already discussed for samples **M(3)** and **M(5)**, that the XPS signal arises mainly from physisorbed molecules.

Through the XPS data analysis, the thickness of the sample films can be estimated, exploiting the correlation between the signal intensity and the coverage thickness. This feature, for an overlayer adsorbed onto a substrate, can be calculated by evaluating the attenuation of the substrate signal according to the equation

$$I = I_0 \exp(-d/\lambda_{Au})$$

where I is the intensity of the substrate signal in the presence of the overlayer, I_0 the intensity of the same signal for the clean surface, d is the overlayer thickness, and λ_{Au} is the inelastic mean free path for gold. λ_{Au} is correlated to the kinetic energy (KE) of the photoemitted electron by equation

$$\lambda_{Au} = B(KE)^{1/2}$$

where $B = 0.087$ nm $(\text{eV})^{-1/2}$ for organic materials.[73] Within the limits of the method and the use of a B factor that is not specifically appropriate, we find that the thickness values calculated in this way for the three SAMs are 0.2, 0.4, and 1.1 nm for samples **SAM(3)**, **SAM(4)**, and **SAM(5)**, respectively, as reported in Table 1. By comparison with molecular dimensions evaluated from the XRD data reported above, these values are indicative for monolayer or submonolayer adsorption regimes, thus excluding the presence of multilayers and in agreement with the expectations.

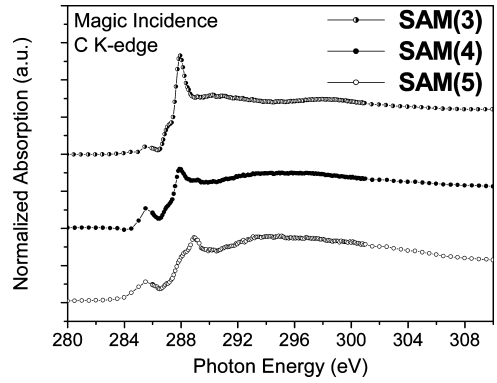

Figure 8. NEXAFS C K-edge spectra of **SAM(3)**, **SAM(4)**, and **SAM(5)** recorded in magic angle geometry.

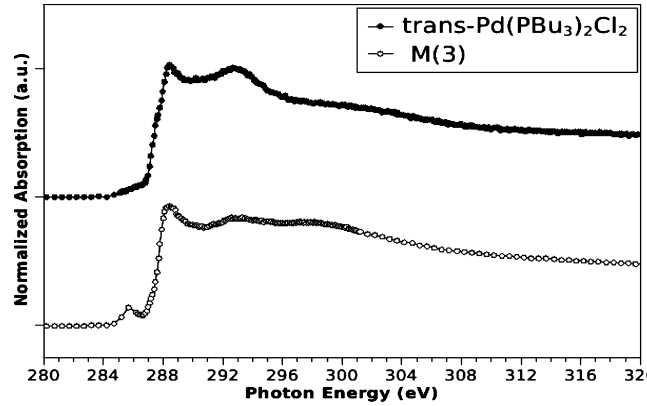

Figure 9. NEXAFS C K-edge spectra of complex trans-$Pd(PBu_3)_2Cl_2$ thick film on gold and of **M(3)** grafted on the same substrate.

3.2.3. NEXAFS Spectra. NEXAFS spectra of SAM systems obtained from samples **3**, **4**, and **5** were acquired at the C K-edge. Measurements were performed by varying the incidence angle of the linearly polarized (95%) synchrotron radiation on the sample surface, from grazing (20°) to normal (90°), with the aim to investigate the electronic structure as well as the average orientation of molecules.

NEXAFS C K-edge spectra of SAMs **3**, **4**, and **5** recorded at an X-ray incidence angle of 54.7° on the substrate (magic incidence), for which the measured intensity distribution is independent of the molecular orientation, are displayed in Figure 8.

The peak assignment of the relevant spectral features can be done by considerations correlated to the chemical structure and comparison with literature data. The chemical structure of molecules grafting the gold surface after depositing sample **3** is strictly similar to the inorganic Pd(II) coordination compound *trans*-$Pd(PBu_3)_2Cl_2$. In Figure 9, the C K-edge NEXAFS spectrum of **M(3)** on gold is displayed; the spectrum measured for the *trans*-$Pd(PBu_3)_2Cl_2$ complex is also reported for comparison. Both spectra show a dominant feature at about 288 eV and a less intense band at 288.90 eV, associated with C1s → σ^* C−H transitions due to the butyl groups, and a broadband around 293 eV assigned to C1s → σ^* C−C excitations of the same butyl phosphyne moieties. The small feature occurring at the low-energy side of the first resonance of the **M(3)** spectrum is thought to be an artifact due to the monochromator; this is not observed in the*trans*-$Pd(PBu_3)_2Cl_2$ complex that was measured in a previous experiment at a different storage ring (LURE-superACO-beamline SA72).

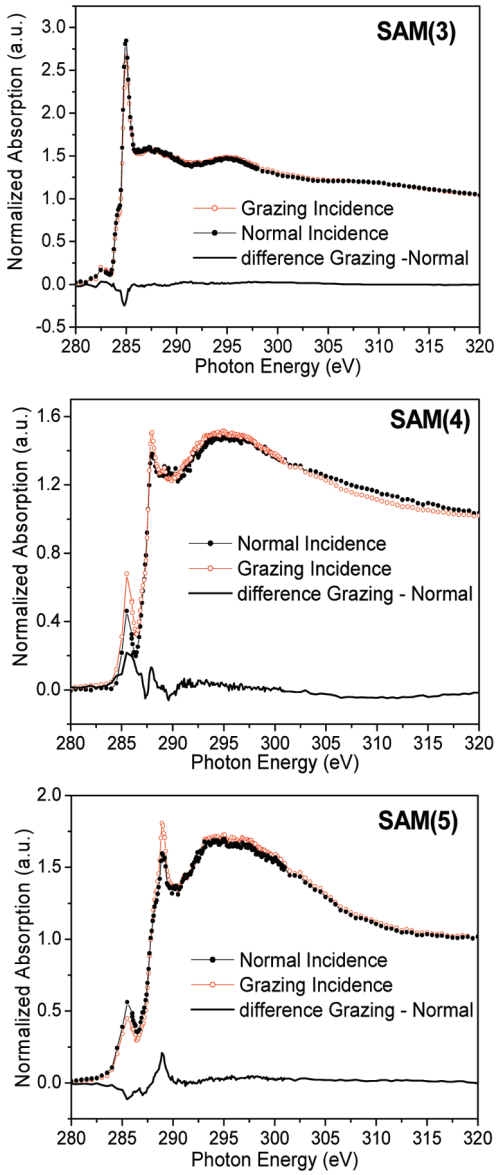

Figure 10. Polarization-dependent NEXAFS C K-edge spectra of **SAM(5)**, **SAM(6)**, and **SAM(7)**. The spectra have been recorded at grazing (20°) (○) and normal (90°) (●) photon incidence angles; the difference spectra (grazing − normal) are also displayed (black lines).

Following a similar approach, the assignment of peaks for the C K-edge spectra of mono and multilayers on gold, obtained from samples **4** and **5**, that are alike due to the analogous chemical groups (Pd−ethynnyl benzene−SH, Pd2-diethynyl biphenyl−$(SH)_2$), can be made by analogy with Pd-DEBP2.[74] The main feature occurring at 285.50 eV is assigned to the superimposition of the nearly unaltered C1s → π^* transition of the benzene ring, due to the ring carbons' not being bonded to the alkyne group and the low energy contribution of the acetylene carbons. The signal at about 286 eV originates from the higher-energy excitation of the alkyne carbons (C≡C) and includes a contribution from the ring carbon bonded to the acetylene functional group. The resonance at nearly 288 eV is related to σ^*C−H due to the butyl groups, and the feature at about 288.90 eV is thought to be derived by the overlapping of a high energy π^* plus σ^*C−H. The broad bands around 293 is assigned to σ^*C−C, and the one at 303 eV is C═C benzene-like. The expected feature above 310 eV, and originating from the σ^*C≡C, did not show up from the spectral background.

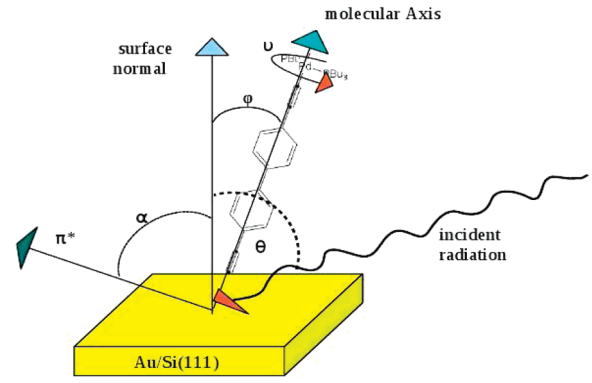

Figure 11. Scheme reporting the angles used to determine the geometrical arrangement of **SAM(4)** and **SAM(5)** on the substrate.

As shown in Figure 10, the C K-edge spectra were acquired at grazing and normal geometry; that is, the incidence angle of the linearly polarized light was varied from 20° to 90°. The NEXAFS resonances intensity depends on the orientation of the transition dipole moment ($\boldsymbol{\mu}$) of the probed molecules relative to the polarization vector (**p**) of the incoming radiation. If the directions of the electric field of the incoming radiation (**E**) and $\boldsymbol{\mu}$ are parallel to each other, the intensity is at the maximum. On the other hand, the excitation does not occur when the vectors **E** and $\boldsymbol{\mu}$ are orthogonal to each other.[75] The intensity of the first and second features observed in the SAM **4** and **5** spectra (see Figure 10) shows a small but clear variation with the beam incidence angle (linear dichroism), suggesting a high level of molecular organization. Sample **SAM(3)** does not show angular dependence effects, as predictable on the basis of its molecular structure.

The average tilt angle of SAMs **4** and **5** (i.e., the angle between the molecular axis and the normal to the substrate) was obtained by the quantitative analysis of the angular dependence of the first π^* resonance (attributed to C 1s−π^* aromatic ring transition) intensity, following the procedure reported by Stöhr.[75] For the **SAM(4)** sample (one EP unit), the average tilt angle was calculated by applying the simple formula

$$I(\theta, \alpha) = 1 + (1/2)(3\cos^2\theta - 1)(3\cos^2\alpha - 1)$$

where angle α is the angle between the π^* vector orbital and the normal to the surface plane (in this case, the average tilt angle of molecular axis, φ, is simply 90° − α), and θ is the incidence angle of the X beam on the sample. A schematic drawing reporting the angles used to determine the molecular arrangement on the substrate is reported in Figure 11.

Molecules of **SAM(5)** contain the DEBP unit in which the two aromatic rings are twisted at an angle of α = 42°[72] with respect to the plane defined by the surface normal and the molecular axis. In this case, a more appropriate formula was used. The term "cos α" can be expressed through the angle ν and the average tilt angle φ of the molecular axis with respect to the normal to the substrate:

$$\cos\alpha = \cos\upsilon \sin\varphi$$

$$I(\theta, \alpha, \upsilon) \sim 1 + (1/2)(3\cos^2\theta - 1)(3\cos^2\theta \sin\varphi - 1)$$

(See ref 29 regarding the latter of the above equations.) Following this procedure, tilt angles, φ, of 40° and 30° were

estimated for **SAM(4)** and **SAM(5)**, respectively; **SAM(5)** appears to attain a more upstanding position on the surface.

Concerning the thickness fo the SAM samples, the evaluated average tilt angles lead to calculated expected values that can be compared to the ones experimentally determined by the HRXPS Au 4f signals' attenuation. Taking an XRD-based length of the molecule (including just the S atom of the terminal thiolate group) d_{XRD} and estimating a S−Au bond length value of 1.8 Å,[29] the organometallic thioles SAM thickness was estimated by

$$d = d_{XRD} \cos \varphi + 1.8$$

obtaining a thickness of 1.8 nm for **SAM(5)** and 1.0 for **SAM(4)**. Since the **SAM(3)** molecules results are not oriented, the same calculation for this system was not performed. These values are overestimated due to the incertitude in tilt angle determination by NEXAFS (about 15% of the estimated angle value) and the approximated XRD molecular lengths; however, they represent the maximum thickness values compatible with a monolayer coverage on the substrate. The comparison with HRXPS data confirms that the procedure followed to produce SAMs leads to substrate coverage degrees of no more than one monolayer.

4. Conclusions

Multilayers and self-assembled monolayers of organometallic thiols in situ prepared starting from organometallic thiolates, that is, *trans*-[$Pd(PBu_3)_2(SCOCH_3)_2$], *trans*-[$(C_6H_5C{\equiv}C)Pd(PBu_3)_2(SCOCH_3)$], and *trans*,*trans*-[$(CH_3COS)Pd(PBu_3)_2(C{\equiv}C-C_6H_4-C_6H_4-C{\equiv}C)(PBu_3)_2Pd(SCOCH_3)$], were deposited onto gold surfaces by a dipping procedure. The self-assembly of the thiols on the gold surface was assessed, and the HR-XPS measurements joined with NEXAFS studies allowed us to evaluate the anchoring of the organometallic moieties through the sulfur linkage to gold. Depending on the investigated molecule, the interaction occurring at the interface and the molecular orientation of the thiols on the surface with tilt angles (defined as the angle between the molecular axis and the normal to the surface) of about 30−40° was observed. The thickness of the obtained SAMs was calculated to be 0.2, 0.4, and 1.1 nm for samples **SAM(3)**, **SAM(4)**, and **SAM(5)**, respectively. By comparison with molecular dimensions evaluated from the XRD data, these values are indicative of monolayer or submonolayer adsorption regimes. NEXAFS studies suggested a high level of molecular organization for SAMs **4** and **5**. These SAMs offer a promising perspective for the applications of these materials in nanoelectronics.

Acknowledgment. The authors gratefully acknowledge the financial support of University La Sapienza "Ateneo 2007".

Supporting Information Available: Chemical synthesis details and XPS characterization data of mono and binuclear Pd(II) complexes, together with crystallographic data table and CIF files for complexes **2**, **3**, and **5** are supplied. This material is available free of charge via the Internet at http://pubs.acs.org.

References and Notes

(1) Park, H. H.; Jamison, A. C.; Lee, T. R. *Nanomedicine* **2007**, *2*, 425.

(2) Love, J. C.; Estroff, L. A.; Kriebel, J. K.; Nuzzo, R. G.; Whitesides, G. M. *Chem. Rev.* **2005**, *105*, 1103.

(3) Kim, M.; Hohman, J. N.; Morin, E. I.; Daniel, T. A.; Weiss, P. S. *J. Phys. Chem. A* **2009**, *113*, 3895.

(4) Heimel, G.; Romaner, L.; Bredas, J. L.; Zojer, E. *Surf. Sci.* **2006**, *600*, 4548.

(5) Halik, M.; Klauk, H.; Zschieschang, U.; Schmid, G.; Dehm, C.; Schutz, M.; Maisch, S.; Effenberger, F.; Brunnbauer, M.; Stellacci, F. *Nature* **2004**, *431*, 963.

(6) Nilsson, D.; Watcharinyanon, S.; Li, L. Q.; Moons, E.; Johansson, L. S. O.; Zharnikov, M.; Shaporenko, A.; Albinsson, B.; Martensson, J. *Langmuir* **2007**, *23*, 6170.

(7) Chechik, V.; Schonherr, H.; Vancso, G. J.; Stirling, C. J. M. *Langmuir* **1998**, *14*, 3003.

(8) Lindsay, S. M.; Ratner, M. A. *Adv. Mater.* **2007**, *19*, 23.

(9) James, D. K.; Tour, J. M. *Chem. Mater.* **2004**, *16*, 4423.

(10) James, P. V.; Sudeep, P. K.; Suresh, C. H.; Thomas, K. G. *J. Phys. Chem. A* **2006**, *110*, 4329.

(11) Greaves, S. J.; Flynn, E. L.; Futcher, E. L.; Wrede, E.; Lydon, D. P.; Low, P. J.; Rutter, S. R.; Beeby, A. *J. Phys. Chem. A* **2006**, *110*, 2114.

(12) Kushmerick, J. G.; Holt, D. B.; Pollack, S. K.; Ratner, M. A.; Yang, J. C.; Schull, T. L.; Naciri, J.; Moore, M. H.; Shashidhar, R. *J. Am. Chem. Soc.* **2002**, *124*, 10654.

(13) Wang, C.; Bryce, M. R.; Gigon, J.; Ashwell, G. J.; Grace, I.; Lambert, C. J. *J. Org. Chem.* **2008**, *73*, 4810.

(14) Wong, W.-Y. *Dalton Trans.* **2007**, 4495.

(15) Wong, W.-Y. *Comments Inorg. Chem.* **2005**, *26*, 39. Wong, W.-Y. *Macromol. Chem. Phys.* **2008**, *209*, 14.

(16) Wong, W.-Y. *Coord. Chem. Rev.* **2005**, *249*, 971.

(17) Wong, W.-Y. *J. Inorg. Organomet. Polym. Mater.* **2005**, *15*, 197. Wong, W.-Y.; Ho, C. L. *Coord. Chem. Rev.* **2006**, *250*, 2627.

(18) Wong, W.-Y. *Coord. Chem. Rev.* **2007**, *251*, 2400.

(19) Long, N. J.; Williams, C. K. *Angew. Chem., Int. Ed.* **2003**, *42*, 2586.

(20) Caliendo, C.; Contini, G.; Fratoddi, I.; Irrera, S.; Pertici, P.; Russo, M. V.; Scavia, G. *Nanotechnology* **2007**, *18*, 125504.

(21) Manners, I. *Synthetic Metal-Containing Polymers*; Wiley-VCH: Weinheim, 2004, chapter 5, p 153.

(22) Fisher, G. L.; Walcher, A. V.; Hooper, A. E.; Tighe, T. B.; Bahnck, K. B.; Scriba, H. T.; Reinard, M. D.; Haynie, B. C.; Opila, R. L.; Winograd, N.; Allara, D. L. *J. Am. Chem. Soc.* **2002**, *124*, 5528.

(23) Chu, B. W. K.; Yam, V. W. W. *Inorg. Chem.* **2001**, *40*, 3324.

(24) De Boer, B.; Meng, H.; Perepichka, D. F.; Zheng, J.; Frank, M. F.; Chabal, Y. J.; Bao, Z. *Langmuir* **2003**, *19*, 4272.

(25) Ying, J. W.; Sobransingh, D. R.; Xu, G. L.; Kaifer, A. E.; Ren, T. *Chem. Commun.* **2005**, 357.

(26) Hempenius, M. A.; Peter, M.; Robins, N. S.; Kooij, E. S.; Vancso, G. J. *Langmuir* **2002**, *18*, 7629.

(27) Carroll, R. L.; Gorman, C. B. *Angew. Chem., Int. Ed.* **2002**, *41*, 4378.

(28) Troisi, A.; Ratner, M. A. *Small* **2006**, *2*, 172.

(29) Nilsson, D.; Watcharinyanon, S.; Eng, M.; Li, L.; Moons, E.; Johansson, L. S. O.; Zharnikov, M.; Shaporenko, A.; Albinsson, B.; Mårtensson, J. *Langmuir* **2007**, *23*, 6170.

(30) Huber, R.; González, M. T.; Wu, S.; Langer, M.; Grunder, S.; Horhoiu, V.; Mayor, M.; Bryce, M. R.; Wang, C.; Jitchati, R.; Schonenberger, C.; Calame, M. *J. Am. Chem. Soc.* **2008**, *130*, 1080.

(31) James, D. K.; Tour, J. M. *Aldrichim. Acta* **2006**, *39*, 47.

(32) Tour, J. M. *Acc. Chem. Res.* **2000**, *33*, 791.

(33) Mayor, M.; von Haenisch, C.; Weber, H. B.; Reichert, J.; Beckmann, D. *Angew. Chem., Int. Ed.* **2002**, *41*, 1183.

(34) Schull, T. L.; Kushmerick, J. G.; Patterson, C. H.; George, C.; Moore, M. H.; Pollack, S. K.; Shashidhar, R. *J. Am. Chem. Soc.* **2003**, *125*, 3202.

(35) Tour, J. M.; Jones, L. R., II.; Pearson, D. L.; Lamba, J. J. S.; Burgin, T. P.; Whitesides, G. M.; Allara, D. L.; Parikh, A. N.; Atre, S. V. *J. Am. Chem. Soc.* **1995**, *117*, 9529.

(36) Zehner, R. W.; Sita, L. R. *Langmuir* **1997**, *13*, 2973. Martin, R. E.; Diederich, F. *Angew. Chem., Int.* **1999**, *38*, 1350.

(37) Vitale, F.; Vitaliano, R.; Battocchio, C.; Fratoddi, I.; Piscopiello, E.; Tapfer, L.; Russo, M. V. *J. Organomet. Chem.* **2008**, *693*, 1043.

(38) Vitale, F.; Vitaliano, R.; Battocchio, C.; Fratoddi, I.; Giannini, C.; Piscopiello, E.; Guagliardi, A.; Cervellino, A.; Polzonetti, G.; Russo, M. V.; Tapfer, L. *Nanoscale Res. Lett.* **2008**, *3*, 461.

(39) Fratoddi, I.; Battocchio, C.; Polzonetti, G.; Mataloni, P.; Russo, M. V.; Furlani, A. *J. Organomet. Chem.* **2003**, *674*, 10.

(40) Beamson, G.; Briggs, D. *High Resolution XPS of Organic Polymers, the Scienta ESCA300 Database*; Wiley: New York, 1992.

(41) Scofield, J. M. *J. Electron Spectrosc. Relat. Phenom.* **1976**, *8*, 129.

(42) Sheldrick, G. M. *SADABS, Program for Empirical Absorption Correction*; University of Göttingen: Germany, 1996.

(43) Altomare, A.; Burla, M. C.; Camalli, M.; Cascarano, G. L.; Giacovazzo, C.; Guagliardi, A.; Moliterni, A. G. G.; Polidori, G.; Spagna, R. J. *Appl. Crystallogr.* **1999**, *32*, 115.

(44) Sheldrick, G. M. *SHELX-97*; University of Göttingen: Göttingen, Germany, 1997.

(45) *Surface Chemical analysis - X-ray photoelectron spectrometers - Calibration of the energy scales; ISO 15472*; International Organization for Standardization: Geneva, Switzerland, 2001.
(46) Shirley, D. A. *Phys. Rev. B* **1972**, *5*, 4709.
(47) Kauffman, G. B.; Teter, L. A. *Inorg. Synth.* **1963**, *7*, 245.
(48) Takahashi, S.; Kuroyama, Y.; Sonogashira, K.; Hagihara, N. *Synthesis* **1980**, 627.
(49) Hagihara, N.; Sonogashira, K.; Takahashi, S. *Adv. Polym. Sci.* **1981**, *41*, 151.
(50) Neo, Y. C.; Vittal, J. J.; Hor, T. S. A. *J. Organomet. Chem.* **2002**, *757*, 637–639.
(51) Cindrić, M.; Vrdoljak, V.; Prugovečki, D.; Kamenar, B. *Polyhedron* **1998**, *17*, 3321.
(52) Robinson, S. D.; Sahajpal, A.; Tocher, D. A. *J. Chem. Soc., Dalton Trans.* **1997**, 757.
(53) Cabri, W.; Candiani, I.; Bedeschi, A. *J. Org. Chem.* **1992**, *57*, 3558.
(54) Xu, L.; Chen, W.; Xiao, J. *Organometallics* **2000**, *19*, 1123.
(55) Ozawa, F.; Kubo, A.; Hayashi, T. *Chem. Lett.* **1992**, *11*, 2177.
(56) Cao, R.; Hong, M.; Jiang, F.; Kang, B.; Xie, X.; Liu, H. *Polyhedron* **1996**, *15*, 2661.
(57) Lai, C.; Backes, B. J. *Tetrahedron Lett.* **2007**, *48*, 3033.
(58) Goodfellow, J. A.; Stephenson, T. A.; Cornock, M. C. *J. Chem. Soc., Dalton Trans.* **1978**, 1195.
(59) Takagi, F.; Seino, H.; Mizobe, Y.; Hidai, M. *Organometallics* **2002**, *21*, 694.
(60) Sadanani, N. D.; Kapoor, P. N.; Kapoor, R. N. *J. Coord. Chem.* **1985**, *14*, 79.
(61) Liu, L.; Poon, S.-Y.; Wong, W.-Y. *J. Organomet. Chem.* **2005**, *690*, 5036.
(62) Onitsuka, K.; Yamamoto, S.; Takahashi, S. *Angew. Chem., Int. Ed.* **1999**, *38*, 174.
(63) Battocchio, C.; D'Acapito, F.; Fratoddi, I.; La Groia, A.; Polzonetti, G.; Roviello, G.; Russo, M. V. *Chem. Phys.* **2006**, *328*, 269.
(64) Porterfield, W. W. *Chimica Inorganica*; Zanichelli: Bologna, Italy, 2001.
(65) Maitlis, P. M.; Espinet, P.; Russel, M. J. H. In *Comprehensive Organometallic Chemistry*; Wilkinson, G., Gordon, F., Stone, A., Abel, E. W., Eds.; Pergamon: New York, 1982; Chapter 38.1.2.4.
(66) Iucci, G.; Infante, G.; Polzonetti, G. *Polymer* **2002**, *43*, 655.
(67) Polzonetti, G.; Iucci, G.; Furlani, C.; Russo, M. V.; Furlani, A.; Infante, G.; Paolucci, G.; Brena, B.; Cocco, D. *Chem. Phys. Lett.* **1997**, *267*, 384.
(68) Contini, G.; Turchini, S.; Di Castro, V.; Polzonetti, G.; Marabini, A. M. *Appl. Surf. Sci.* **1992**, *59*, 1.
(69) Dubois, L. H.; Nuzzo, R. G. *Annu. Rev. Phys. Chem.* **1992**, *43*, 437.
(70) Bethencourt, M. I.; Srisombat, L.; Chinwangso, P.; Lee, T. R. *Langmuir* **2009**, *25*, 1265.
(71) Bensebaa, F.; Yu, Z.; Deslandes, Y.; Kruus, E.; Ellis, T. H. *Surf. Sci.* **1998**, *405*, L472.
(72) Campbell, C. T.; Koel, B. E. *Surf. Sci.* **1987**, *183*, 100.
(73) Swift, P.; Shuttleworth, D.; Seah, M. P. *Practical Surface Analysis by Auger and X-ray Photoelectron Spectroscopy*; Briggs D., Seah, M. P., Eds.; J. Wiley & Sons: Chichester, 1983; chapter 4.
(74) Battocchio, C.; Fratoddi, I.; Russo, M. V.; Carravetta, V.; Monti, S.; Iucci, G.; Borgatti, F.; Polzonetti, G. *Surf. Sci.* **2007**, *601*, 3943.
(75) Stöhr, J. *NEXAFS Spectroscopy*; Springer Series in Surface Sciences; Geomer, R., Ed.; Springer-Verlag: New York, 1991; Chapter 9.4.3.
(76) Carravetta, V.; Iucci, G.; Ferri, A.; Russo, M. V.; Stranges, S.; De Simone, M.; Polzonetti, G. *Chem. Phys.* **2001**, *264*, 175.

JP904865K